

## Corrosion Characteristics of Ammonium Bisulfate, an SCR Denitrification By-product, on Boiler Tail-end Metal Materials (Postprint)

**Authors:** Ma Shuangchen, Deng Yue, Wu Wenlong, Tan Yu, Zhang Linan, Chai Feng, Sun Panpan, Zhang Xiaoni

**Date:** 2016-11-07T00:00:00+00:00

### Abstract

The corrosion behavior of boiler tail-end materials—carbon steel and stainless steel—in ABS (ammonium bisulfate) and H<sub>2</sub>SO<sub>4</sub> solutions was investigated through static weight loss experiments, with corrosion characteristics analyzed via potentiodynamic polarization curves. The findings reveal that carbon steel and stainless steel exhibit similar corrosion processes in ABS and sulfuric acid solutions of equivalent concentration, demonstrating that ABS possesses strong corrosivity. Corrosion products were characterized using SEM/EDS and XPS. Observation of the SEM morphology of corrosion product surface layers on carbon steel and stainless steel in ABS solutions of varying concentrations indicates that stainless steel demonstrates superior corrosion resistance to ABS, with corrosion severity intensifying as ABS solution concentration increases. EDS and XPS analyses of the corrosion product film yielded the elemental composition and chemical states within the film, ultimately identifying the corrosion products as Fe<sub>2</sub>O<sub>3</sub>, Fe(OOH), Fe<sub>3</sub>O<sub>4</sub>, and iron sulfates. Due to the acidic nature of ABS, acidic corrosion initially occurs on the carbon steel surface, with hydrogen ions serving as depolarizers and hydrogen gas evolution occurring. As acidity is consumed, oxygen corrosion transpires on the metal surface, with dissolved oxygen acting as the depolarizer. Fe<sup>2+</sup> is subsequently further oxidized to Fe<sup>3+</sup>, followed by a series of secondary reactions that generate iron oxides, sulfates, and other compounds.

## Full Text

### Corrosion of Downstream Boiler Metallic Materials by Ammonium Bisulfate, a Byproduct of SCR Denitrification

Deng Yue<sup>1</sup>, Wu Wenlong<sup>2</sup>, Tan Yu<sup>1</sup>, Zhang Linan<sup>1</sup>, Chai Feng<sup>1</sup>, Sun Panpan<sup>1</sup>, Zhang Xiaoni<sup>2</sup>, Ma Shuangchen<sup>1</sup> <sup>1</sup>College of Environmental Science and Engineering, North China Electric Power University, Baoding 071003, China <sup>2</sup>Electric Power Test and Research Institute of State Grid Henan Electric Power Company, Zhengzhou 450052, China

## Abstract

The corrosion behavior of carbon steel and stainless steel—typical materials used in downstream boiler sections—was investigated in ammonium bisulfate (ABS) and H<sub>2</sub>SO<sub>4</sub> solutions using static weight loss experiments. Potentiodynamic polarization curves were employed to analyze corrosion characteristics, while SEM/EDS and XPS were used to characterize the morphology, elemental composition, and chemical states of corrosion products. The results demonstrate that stainless steel exhibits superior corrosion resistance to ABS compared to carbon steel, with corrosion intensity increasing as ABS solution concentration rises. Corrosion products identified include Fe<sub>2</sub>O<sub>3</sub>, FeOOH, Fe<sub>3</sub>O<sub>4</sub>, and iron sulfates. The similar corrosion processes observed for both carbon and stainless steels in equimolar ABS and sulfuric acid solutions indicate that ABS possesses strong corrosive properties analogous to sulfuric acid. The corrosion mechanism proceeds as follows: initial acidic corrosion occurs on the carbon steel surface with H<sub>2</sub> acting as the depolarizing agent, resulting in hydrogen evolution. As acidity is consumed, oxygen corrosion initiates on the metal surface with dissolved oxygen serving as the depolarizer. Fe<sup>2+</sup> is subsequently oxidized to Fe<sup>3+</sup>, triggering a series of secondary reactions that generate iron oxides and sulfates.

**Keywords:** SCR; ammonium bisulfate; H<sub>2</sub>SO<sub>4</sub>; weight loss method; corrosion characteristics

## Introduction

Metallic materials such as carbon steel and stainless steel are widely employed in modern power plants, where they suffer severe corrosion due to high temperature, high pressure, and poor water quality conditions. Selective catalytic reduction (SCR) denitrification has been extensively adopted because of its mature technology and high NO<sub>x</sub> removal efficiency [1-3]. The key component of NH<sub>3</sub>-SCR technology is the SCR catalyst, which typically contains 0.5-4% V<sub>2</sub>O<sub>5</sub> in commercial formulations [4-6]. During flue gas denitrification, the V<sub>2</sub>O<sub>5</sub> catalyst not only reduces NO<sub>x</sub> but also oxidizes a portion of SO<sub>2</sub> to SO<sub>3</sub>. This SO<sub>3</sub> subsequently reacts with unreacted ammonia from the SCR process under certain conditions to form ammonium bisulfate (ABS). ABS is a colorless crystalline substance at room temperature that is highly hygroscopic and readily soluble

in water, forming a strongly acidic solution that can directly ionize H through a dissociation reaction similar to H SO . With a melting point of 147°C, boiling point of 350°C, and density of 1.79 g/mL, this uncommon ammonium salt creates numerous operational problems in SCR systems, including deposition on catalyst surfaces and downstream equipment that causes blockage, corrosion, and increased system resistance [3]. Despite these issues, no studies have yet investigated the corrosion behavior of ABS on metallic materials. Understanding the electrochemical corrosion mechanism of ABS is therefore urgently needed. Since both ABS and H SO can ionize H and SO<sup>2-</sup>, this study employs static weight loss experiments to compare corrosion rates of downstream boiler materials (carbon steel and stainless steel) in these two solutions. SEM/EDS and XPS analyses characterize the elemental composition and chemical states of corrosion product films to identify product species. Combined with potentiodynamic polarization curves, the corrosion mechanism is elucidated, providing theoretical basis and data support for material selection and life assessment under ABS corrosion conditions.

## Experimental Methods

### Materials and Sample Preparation

The experimental materials were 20# carbon steel and 304 stainless steel samples with chemical compositions shown in . Corrosion test coupons measured 10 mm × 10 mm × 3 mm. Samples were annealed after wire cutting, progressively ground to 800# grit using SiC sandpaper, marked with steel stamps for identification, rinsed with deionized water, degreased with acetone, and dried.

### Weight Loss Measurements

Samples were immersed in test solutions according to their numbering for an experimental period of 60 days. After testing, coupons were removed and cleaned in 12% HCl + 2% hexamethylenetetramine at room temperature to remove all corrosion products. Cleaned samples were rapidly rinsed with deionized water, wiped with absolute alcohol, degreased with acetone, dried for 24 hours, and weighed. The average corrosion rate was calculated using the following formula:

$$v = \frac{m_0 - m_1}{S \times t}$$

where  $S$  is the sample area (m<sup>2</sup>),  $t$  is the test duration (h),  $m_0$  is the initial mass (g), and  $m_1$  is the mass after corrosion and cleaning (g).

### Potentiodynamic Polarization Curve Testing

Polarization measurements employed a standard three-electrode system with the test sample as the working electrode, Pt as the counter electrode, and saturated calomel electrode (SCE) as the reference electrode [7-9]. The Tafel line

extrapolation method was used, where the linear Tafel regions of the anodic and cathodic polarization curves were extrapolated to intersect at a point corresponding to the corrosion potential ( $E_{\text{corr}}$ ) and corrosion current density ( $I_{\text{corr}}$ ) [10-12].

Metal electrodes were prepared by machining 20# carbon steel and 304 stainless steel into 10 mm × 10 mm × 3 mm samples, progressively ground from 100# to 1000# grit, and polished. Samples were cleaned with deionized water, degreased with acetone, and dried. Fine copper wires were soldered to the sample surfaces, which were then encapsulated in epoxy resin. After 24 hours of curing, the encapsulated samples were ground and polished. A 100 mL aliquot of prepared solution was transferred to a three-neck flask, and the Pt electrode, SCE, and test sample were connected to a multi-channel potentiostat/galvanostat. Polarization curves were measured after open-circuit potential stabilization using a scan rate of 0.3 mV/s.

### Corrosion Product Characterization

Surface morphology and corrosion product composition were examined using a BRUKER Nano X Flash Detector 5010 SEM equipped with EDS (Genesis 2000). A PHI5000 XPS system was employed to analyze the elemental composition and chemical states of corrosion product films, using Mg K radiation at 300 W, 89.45 eV for full-element scanning, 71.55 eV for single-element scanning, and C 1s = 284.8 eV for binding energy calibration.

## Results and Discussion

### Corrosion Morphology Observations

Visual examination revealed that samples in sulfuric acid solution developed uniform brown corrosion products with black residues in solution, while those in ABS solution formed uniform dark yellow corrosion products. Higher solution concentrations produced more corrosion products in both cases. [Figure 1: see original paper] shows SEM images of carbon steel corrosion films: Figure 1a in 3000 mg/L ABS solution and Figure 1b in 3000 mg/L H<sub>2</sub>SO<sub>4</sub> solution. Comparison indicates that ABS-exposed samples developed a thin oxide scale with small corrosion pits, whereas H<sub>2</sub>SO<sub>4</sub>-exposed samples exhibited distinct corrosion cracks, demonstrating more severe corrosion of 20# carbon steel in sulfuric acid at equivalent concentrations. [Figure 2: see original paper] presents the corrosion morphology of stainless steel in 3000 mg/L ABS solution, showing a relatively uniform and smooth surface without obvious impurities, pores, or corrosion traces, confirming superior corrosion resistance.

### Corrosion Rate Calculations

Corrosion rates for carbon steel and stainless steel in various solutions were calculated using the weight loss formula, with results summarized in and . [Figure

3: see original paper] illustrates the corrosion rates of carbon steel in different ABS and sulfuric acid concentrations. Compared to blank experiments, corrosion rates increased with solution concentration for both ABS and H<sub>2</sub>SO<sub>4</sub>. At equivalent concentrations, carbon steel corroded faster in sulfuric acid than in ABS solution. [Figure 4: see original paper] shows stainless steel corrosion rates, revealing that higher concentrations accelerated corrosion. At low concentrations, stainless steel corroded faster in sulfuric acid, but at high concentrations, the rates became similar. Stainless steel exhibited significantly lower corrosion rates than carbon steel in both solutions.

[Figure 5: see original paper] presents EDS spectra of carbon steel after 60 days immersion in 3000 and 30000 mg/L ABS solutions. The analysis regions primarily contained O, S, and Fe–Fe from the carbon steel, S from ABS solution, and O mainly from dissolved oxygen. Higher ABS concentrations yielded higher S content in corrosion products, indicating more severe corrosion.

### Potentiodynamic Polarization Behavior

Tafel slope fitting of polarization curves yielded corrosion potentials ( $E_{\text{corr}}$ ) of -0.796, -0.657, and -0.609 V for carbon steel in 300, 3000, and 30000 mg/L ABS solutions, respectively, with corresponding corrosion current densities ( $I_{\text{corr}}$ ) of 50.119, 112.202, and 851.140 A · cm<sup>2</sup>. This demonstrates that increasing ABS concentration accelerates carbon steel corrosion. [Figure 7: see original paper] shows polarization curves for carbon steel in 3000 mg/L ABS and sulfuric acid solutions, which exhibit high similarity. Tafel fitting reveals comparable  $E_{\text{corr}}$  and  $I_{\text{corr}}$  values, with slightly higher values in sulfuric acid, indicating similar corrosion severity with marginally faster rates in H<sub>2</sub>SO<sub>4</sub>.

[Figure 8: see original paper] and [Figure 9: see original paper] show polarization curves for stainless steel in ABS and sulfuric acid solutions. In three ABS concentrations, curves transition from activation polarization to active-passive transition, then to stable passivation. Above 0.8 V, stainless steel enters the transpassive region where the passive film breaks down and current density increases sharply. More negative  $E_{\text{corr}}$  and higher  $I_{\text{corr}}$  in 3000 and 30000 mg/L ABS compared to 300 mg/L indicate accelerated corrosion at high concentrations, though rates in 3000 and 30000 mg/L solutions are similar, consistent with weight loss results. Stainless steel shows comparable  $E_{\text{corr}}$  and  $I_{\text{corr}}$  in 3000 mg/L ABS and sulfuric acid solutions, with similar corrosion processes despite a longer activation region in H<sub>2</sub>SO<sub>4</sub>, suggesting equivalent corrosive effects at equal concentrations.

The corrosion mechanism involves rapid Fe dissolution when active, but the presence of abundant SO<sub>4</sub><sup>2-</sup> leads to FeSO<sub>4</sub> precipitation that blocks the anodic reaction, limiting diffusion current density. Since H<sup>+</sup> cannot easily penetrate the FeSO<sub>4</sub> layer, pH increases and Fe<sub>2</sub>O<sub>3</sub> begins forming on the surface above -0.5 V, creating a dense oxide film that causes passivation. This passive state persists until the potential exceeds the O<sub>2</sub>/H<sub>2</sub>O equilibrium potential, when

oxygen evolution begins and current density increases again.

### XPS Analysis of Corrosion Product Films

Full-element XPS scans provide binding energy spectra for different electron subshells, revealing film composition. [Figure 10: see original paper] shows full XPS spectra of carbon steel corrosion products after 60 days in 300 and 30000 mg/L ABS solutions. The 300 mg/L spectrum shows Fe, C, and O—Fe from the steel, C from steel and medium, and O from the corrosive medium—indicating the film consists primarily of Fe oxides, carbonates, mixed salts, or their combinations. The 30000 mg/L spectrum shows Fe, C, O, and S, with S appearing only at high concentration, confirming ABS participation in corrosion at high concentrations but minimal effect at low concentrations. Narrow scans of each element provide oxidation states for final composition determination.

[Figure 11: see original paper] shows elemental peaks for carbon steel corrosion films in 300 and 30000 mg/L ABS solutions. C 1s spectra exhibit three-component peaks: 285.34 eV (low concentration) and 285.36 eV (high concentration) correspond to C-O ( 285.40 eV); 285.01 eV (low) and 284.95 eV (high) correspond to elemental carbon ( 285.10 eV); and 284.57 eV (low) and 284.39 eV (high) correspond to crystalline graphite ( 284.50 eV), likely from air adsorption or contamination rather than corrosion products. O 1s shows three-component overlapping peaks at low concentration and two separate peaks at high concentration. The main absorption peaks at 531.18 and 531.55 eV correspond to Fe O ( 531.10 eV), while peaks at 530.38 eV (low) and 530.28 eV (high) correspond to OH ( 530.50 eV), and the lowest energy peak at 529.97 eV (low concentration) corresponds to FeO ( 529.80 eV).

Fe 2p spectra show main peaks at 712.66 and 712.46 eV corresponding to FeOOH, peaks at 710.81 eV (low) and 710.96 eV (high) corresponding to Fe O ( 710.80 eV), and a peak at 710.46 eV (high concentration) corresponding to Fe O ( 710.50 eV). S 2p peaks at 169.53, 168.72, and 168.37 eV correspond to Fe (SO ) , FeSO , and Na SO , respectively.

These results indicate that carbon steel corrosion films after 60 days in 300 mg/L ABS contain Fe O and FeOOH, while films formed in 30000 mg/L ABS contain Fe O , FeOOH, Fe O , and iron sulfates.

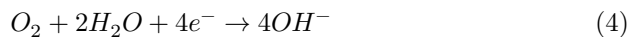
The corrosion mechanism proceeds as follows: ABS solutions are acidic, causing general corrosion on carbon steel surfaces. The overall process comprises cathodic depolarization reduction and anodic metal oxidation. Initially, hydrogen depolarization corrosion occurs:



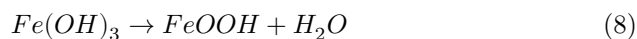
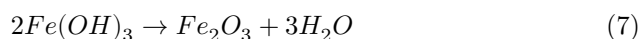
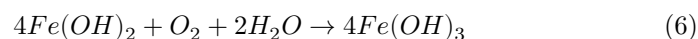
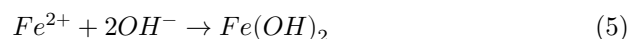
The anodic reaction is active metal dissolution:



As H is consumed and dissolved oxygen acts, oxygen depolarization corrosion begins:



Secondary reactions between  $Fe^{2+}$  and  $OH^{-}$  produce:



In ABS solutions,  $SO^{2-}$  participates in reactions to form iron sulfates, though at 300 mg/L the low  $SO^{2-}$  concentration yields minimal sulfate content.

## Conclusions

- (1) The similar corrosion processes of 20# carbon steel and 304 stainless steel in various concentrations of ABS and sulfuric acid solutions demonstrate that ABS exhibits acidic characteristics with strong corrosivity.
- (2) Morphological observations reveal that stainless steel possesses better corrosion resistance to ABS than carbon steel, with corrosion intensity increasing as ABS solution concentration rises.
- (3) SEM/EDS and XPS analyses of corrosion product films formed on carbon steel and stainless steel after 60 days in two ABS concentrations identified the corrosion products as  $FeO$ ,  $FeOOH$ ,  $Fe_2O_3$ , and iron sulfates.
- (4) The corrosion mechanism of ABS on carbon steel resembles that of sulfuric acid. Due to its acidity, initial hydrogen depolarization corrosion occurs on the carbon steel surface with  $H_2$  evolution. As acidity is consumed and dissolved oxygen acts, oxygen depolarization corrosion proceeds.  $Fe^{2+}$  is further oxidized to  $Fe^{3+}$ , initiating secondary reactions that generate iron oxides and sulfates.

## References

- [1] Long X L, Xin Z L, Wang H X, Xiao W D, et al. Simultaneous removal of NO and SO<sub>2</sub> with hexamminecobalt solution coupled with the hexamminecobalt(II) regeneration catalyzed by activated carbon, *Applied Catalysis B: Environmental* 2004,54:25-32
- [2] Ma S C, Jin X, Sun Y X, et al. The formation mechanism of ammonium bisulfate in SCR flue gas denitrification process and control[J]. *Thermal Power Generation*, 2010, 39(8):
- [3] Ma S C, Guo M, Song H H, et al. Formation mechanism and influencing factors of ammonium bisulfate during the selective catalytic reduction process[J]. *Thermal Power Generation*, 2014,43(2):75-78
- [4] Xiong Z B, Lu C M, Han K H, et al. Effect of precipitants on selective catalytic reduction of NO<sub>x</sub> by NH<sub>3</sub> over iron-cerium mixed metal oxide catalyst[J]. *Journal of China Coal Society*, 2013,38(1):201-205
- [5] Liu F D, Shan W P, Shi X Y, et al. Vanadium-Based Catalysts for the Selective Catalytic Reduction of NO<sub>x</sub> with NH<sub>3</sub> [J]. *Progress In Chemistry*, 2012,24(4):446-455
- [6] Gildas G, Kamel B, Nadia H, et al. The corrosion protection behavior of zinc rich epoxy paint in 3%NaCl solution [J]. *Adv. Chem. Eng. Sci.*, 2011, 1(2): 51
- [7] Tan Y, Liang K X, Zhang S H. Semiconductor properties of the passive film formed on Ni201 in neutral solution[J]. *Journal of Chinese Society for Corrosion and Protection*, 2012,48(8):971-976
- [8] Nagarajan S, Karthega M, Rajendran N. *J Appl Electrochem*, 2007,37:195.
- [9] Zhou J L, Li X G, Du C W, et al. Anodic electrochemical behavior of X80 pipeline steel in NaHCO<sub>3</sub> solution[J]. *Acta Metallurgica Sinica*, 2010,46(2):251-256
- [10] Wang J Y, Kong X D. Electrochemical corrosion behavior of two Al-based Alloys in 3% NaCl solution[J]. *Corrosion Science and Protection Technology*, 2011,23(1):41-44
- [11] Chen F, Xie L X, Sun C, et al. Study the corrosion phenomenon of aluminum alloy the seawater by potentiodynamic polarization curve method[J]. *Tianjin Chemical Industry*, 2014, 28(5): 12-14
- [12] Yue C B, Fang D, Liu L, et al. Synthesis and application of task-specific ionic liquids used as catalysts and/or solvents in organic unit reactions [J]. *J. Mol. Liq.*, 2011, 163(3): 99

*Note: Figure translations are in progress. See original paper for figures.*

*Source: ChinaXiv – Machine translation. Verify with original.*